Journal Name

ARTICLE TYPE

Cite this: DOI: 00.0000/xxxxxxxxxx

Positive Feedback Drives A Secondary Nonlinear Product Burst During a Biphasic DNA Amplification Reaction†

Burcu Özay,[a‡] Shannon D. Murphy,[b‡] Esther E. Stopps,[a] Tomáš Gedeon,[b] and Stephanie E. McCalla*[a]

Received Date
Accepted Date

DOI: 00.0000/xxxxxxxxxx

Isothermal DNA amplification reactions are used in a broad variety of applications, from diagnostic assays to DNA circuits, with greater speed and less complexity than established PCR technologies. We recently reported a unique, high gain, biphasic isothermal DNA amplification reaction, called the Ultrasensitive DNA Amplification Reaction (UDAR). Here we present a detailed analysis of the UDAR reaction pathways that initiates with a first phase followed by a nonlinear product burst, which is caused by an autocatalytic secondary reaction. The experimental reaction output was reproduced using an ordinary differential equation model based on detailed reaction mechanisms. This model provides insight on the the relative importance of each reaction mechanism during both phases, which could aid in the design of product output during DNA amplification reactions.

1 Introduction

Isothermal amplification reactions have gained popularity over the last two decades with their simplicity and speed, offering improvements in molecular identification[1]. Specifically, these amplification technologies assist in clinical diagnostics, environmental monitoring, and forensic testing, with capabilities similar to standard PCR but with simplified reactions or equipment[2–5]. While these new technologies provide advantages over traditional methods, they are limited by nonspecific amplification and rapid, uncontrolled growth in product formation[6]. Furthermore, these amplification technologies can be more difficult to calibrate and control when compared to PCR as they contain many simultaneous interlinked reaction pathways[7]. These limitations can be overcome with optimization or strategic manipulation of the reaction output. Kinetic modeling aided in optimization and application of PCR technologies[8–10]. The same strategy benefits isothermal DNA amplification applications; mathematical modeling of reaction output is an important tool to determine methods to manipulate or modify the reaction, provide insights on reaction mechanisms, and provide strategies to use these reactions within larger systems such as DNA computing.

Kinetic modeling has already provided clear benefits for both characterization and optimization of isothermal amplification reactions. Exponential Amplification Reaction (EXPAR) produces an output curve very similar to PCR through a process in which a trigger binds a synthetic template with a nicking endonuclease site. In the presence of a polymerase and nicking endonuclease, repeated elongation and nicking amplify the trigger molecule. Van Ness et al.[11] predicted EXPAR output using their mass-action kinetics model and numerically confirmed the exponential nature of EXPAR output. Chen et al.[12] was able to analyze the effect of target molecule hybridization efficiency on EXPAR performance using a mathematical model, where they predicted that 50% hybridization efficiency drops the amplification factor to 1.5 from 2. Moody et al.[13] used mathematical modeling to identify rate limiting steps, effects of stirring, and ability to quantify initial DNA concentration when using Recombinase Polymerase Amplification (RPA). Mathematical analysis of Loop Mediated Amplification (LAMP) reactions improved primer design and reaction efficiency[14,15], which can accelerate assay development. Others used LAMP models to predict product lengths[16,17], which can allow identification of specific amplification[16] or elucidate complex reaction pathways[17]. Mathematical models also simplified analysis of reaction output and provided a mechanism to rapidly analyze amplification output without subjective bias[15].

In addition to molecular detection, nucleic acid-based tool development also used mathematical modeling to design molecular networks, which often include nucleic acids and enzymes. Montagne et al. benefited from establishing a mathematical model for their DNA oscillator, which helped assess the conditions needed

[a] PO Box 173920, Department of Chemical and Biological Engineering, Bozeman, MT, USA. Tel: +1-406-994-2286; E-mail: stephanie.mccalla@montana.edu
[b] P.O. Box 172400, Department of Mathematical Sciences, Bozeman, MT, USA.
* corresponding author Tel: +1-406-994-2286; E-mail: stephanie.mccalla@montana.edu
‡ These authors contributed equally to this work
† Electronic Supplementary Information (ESI) available: [details of any supplementary information available should be included here]. See DOI: 00.0000/00000000.

for stable oscillators[18]. Zhang et al. presented a method to engineer DNA triggered, entropy-driven reactions and networks, using a mathematical model to predict potential outcomes of alterations in their systems[19].

We recently reported on a new DNA amplification method, ultrasensitive DNA amplification reaction (UDAR), which is distinguished from EXPAR by the use of a palindromic template. The palindrome is located both on the 3' end of the trigger and repeated in the template, causing the template to fold in a looped configuration and allowing triggers to weakly dimerize (Fig. 1). While the first phase of UDAR resembles an EXPAR reaction, the addition of a palindrome in the templates leads to a secondary rise in reaction product[20] (Fig. 1A), which can be either steep (type I templates) or gradual (type II templates). Unlike EXPAR, UDAR can therefore produce much greater fluorescence, as well as a variety of unique nonlinear fluorescence outputs. This includes large, switch-like jumps of fluorescence output that are not seen in EXPAR. While distinctive, biphasic DNA amplification characteristics are straightforward to observe experimentally, the complete understanding of the relative effect of each reaction mechanism is still lacking. The original work showed a range of potential reaction outputs from a variety of templates, but did not include a detailed kinetic or mathematical analysis of the reaction. There is not currently a mathematical model to reproduce the steep, switch-like DNA amplification output seen for type I templates, which show a distinct separation between the two amplification phases and sharp second rise of amplification products.

In our previous work, we developed a mathematical model that reproduced the second rise as measured by the fluorescence output of a Type II UDAR template[21]. The original model hypothesized that the templates deactivate with time, but can be recycled by the subsequent binding by one of the reaction products. However, this mechanism was unable to reproduce the sharp second rise seen in Type I templates. While this previous work assumed output fluorescence correlated with total DNA production, we have since found that the fluorescent signal of each reaction product significantly differ; single-stranded DNA staining dye SYBR Green II was not efficient to monitor the short EXPAR and UDAR products at the amplification temperature, which are ten nucleotides long and single stranded. The reactions were therefore not terminating at the plateau, rather the fluorescence was terminating. Therefore, a new experimental approach is required to separately monitor the dominant reaction products and build a new mathematical model of UDAR based on updated reaction mechanisms.

In this work, we quantified the two main reaction products of UDAR using quantitative PAGE over time during both a full UDAR reaction and a reaction reproducing the second phase of type I UDAR templates. Short, single stranded products did not produce significant fluorescence at the reaction temperature, despite using a single-stranded DNA dye. We additionally investigated the affect of a slow deactivation of the nickase enzyme on the reaction. Together, this data established the dominant reaction mechanisms for type I UDAR templates' distinctive product output and supported an alternative hypothesis for the second rise of UDAR. Under this hypothesis the second rise is due to the autocatalytic transformation of single stranded initial products to highly fluorescent double stranded secondary products. Based on these hypothesised reaction mechanisms, we created a mathematical model that can reproduce the measured product output of UDAR reactions. We obtain the parameters directly from experiments, from the enzyme manufacturer, or from a software package that computes dissociation constants for DNA strands[22]. This model can fit the output of two dominant reaction products for three separate templates, which further supports the hypothesis that the second phase signal burst is due to an autocatalytic production of the secondary product. We then examine sensitivity of major features of the amplification process as a function of the parameters. UDAR is a unique example of a DNA amplification reaction that can produce a nonlinear signal burst. This work shows the dominant mechanisms that drive UDAR's nonlinear second phase signal burst, which is uncommon in DNA amplification reactions, and provides insight on how to manipulate the reaction output. Oligonucleotides, including UDAR triggers, can be created in the presence of molecules such as proteins[23–26] and RNA[27,28]. Therefore, the palindromic trigger molecules shown in this work can be specifically created in the presence of a variety of targets, enabling reactions specific to a target of choice that produce a bright, switch-like fluorescence output that differs from existing DNA amplification reactions. This flexibility makes UDAR useful for broad applications such as molecular detection and DNA circuits or DNA logic devices[29].

2 Experimental

2.1 Reagents

10× ThermoPol® Reaction Buffer, Deoxynucleotide (dNTP) Solution Mix, BSA, $MgSO_4$, Nt·BstNBI and Bst 2.0 WarmStart® DNA Polymerase were purchased from NEB (Ipswich, MA). Enzyme concentrations were estimated from specific activities and molecular weights provded by the manufacturer. Ambion® Buffer Kit (Tris-HCl and KCl), SYBR™ Green II RNA Gel Stain, SYBR™ Gold Nucleic Acid Gel Stain and Novex™ TBE-Urea Sample Buffer (2×) were purchased from Thermo Fisher Scientific (Waltham, MA). Glycerol was purchased from Sigma (Burlington, MA). The UDAR templates, 10/60 DNA ladder, nuclease-free water and 1× TE buffer were purchased from IDT (Coralville, IA). The triggers were purchased from Eurofins Genomics (Louisville, KY). Oligonucleotide sequences can be found in the ESI (Table SI 1). 40% Acrylamide/Bis Solution, 29:1, Ammonium Persulfate (APS) and Urea were purchased from Bio-Rad (Hercules, CA). TEMED (Tetramethylethylenediamine) was purchased from Bio Basic Inc. (Amherst, NY). 10× TBE Buffer Concentrate (0.89 M Tris, 0.89 M boric acid, 20 mM EDTA, pH 8.3) was purchased from IBI Scientific (Dubuque, IA).

2.2 Oligonucleotide concentration measurements

Oligonucleotides were quantified using Nanodrop 1000 Spectrophotometer, using nucleic acid application module. 1× TE buffer was used as blank and the Sample Type was arranged to "Other", where the extinction coefficient was set according to each specific sequence. The extinction coefficient (μg/OD)

for each oligonucleotide was obtained from the manufacturer's data sheets. The concentration calculations were conducted using Beer's Law.

2.3 SYBR Green II affinity experiments

Varying concentrations of phosphorylated triggers and phosphorylated dimers associated with all three template types were diluted in UDAR reaction mixture that did not contain template and enzymes, with 10 μL volume and three experimental replicates. The samples were incubated at 55°C for 1 hour, and fluorescence was measured every 32 or 34 seconds for 1 hr in a Bio-Rad CFX Real-Time thermocycler to ensure a stable fluorescent signal.

2.4 Enzyme activity analysis

EXPAR reaction mix contained 1× ThermoPol I Buffer (20 mM Tris-HCl, 10 mM $(NH_4)_2SO_4$, 10 mM KCl, 2 mM $MgSO_4$, 0.1% Triton® X-100, pH 8.8 at 25°C) supplemented with 25 mM Tris-HCl (pH 8.0), 6 mM $MgSO_4$, 50 mM KCl, 0.5 mM each dNTPs, 0.1 mg·mL^{-1} BSA, 0.2 U·μL^{-1} Nt·BstNBI, 0.0267 U·μL^{-1} Bst 2.0 WarmStart® DNA Polymerase, 4× SYBR Green II, 100 nM EXPAR template and 10 pM EXPAR trigger. To test the effect of 55°C incubation on Nt·BstNBI restriction enzyme activity, the reaction was prepared without the polymerase, templates and triggers and distributed into 7 low-profile PCR tubes with 20 μL volume each. The samples were incubated at 55°C for 0, 10, 20, 30, 40, 50 and 60 minutes, and placed on ice for the remaining duration of 60 minutes when not incubated at an elevated temperature. Once the incubations were completed, polymerase, templates and triggers were added to the samples and mixed well. The reactions were incubated in a Bio-Rad CFX Connect thermocycler where real-time fluorescence readings were collected every 22 seconds (including the imaging time) for 164 cycles at 55°C. The same procedure was repeated for testing the effect of 55°C incubation on Bst 2.0 WarmStart® DNA Polymerase activity, this time preparing the samples including the polymerase and taking out the nickase, templates and triggers.

2.5 UDAR and second phase time series experiments

UDAR reaction mix contained 1× ThermoPol® I Buffer (20 mM Tris-HCl, 10 mM $(NH_4)_2SO_4$, 10 mM KCl, 2 mM $MgSO_4$, 0.1% Triton® X-100, pH 8.8 at 25°C) supplemented with 25 mM Tris-HCl (pH 8), 6 mM $MgSO_4$, 50 mM KCl, 0.5 mM each dNTPs, 0.1 mg·mL^{-1} BSA, 6.08% glycerol (to improve stability and repeatability of the reaction), 0.2 U·μL^{-1} Nt·BstNBI, 0.0267 U·μL^{-1} Bst 2.0 WarmStart® DNA Polymerase, 4× SYBR Green II, 100 nM UDAR template and 10 pM trigger. The reaction mix was prepared at 4°C and divided into low-profile, transparent PCR tubes with 20 μL volume each. The samples were incubated in a thermocycler at 55°C and were removed at the specified time points for product analysis. To immediately stop the reaction, the samples were removed from the thermocycler and immediately placed into a Bio-Rad T100 Thermal Cycler at 80°C and incubated for 20 minutes to fully deactivate both enzymes. Three samples were incubated in a Bio-Rad CFX Connect thermocycler to monitor the samples in real time as a reference; real-time fluorescence readings were collected for 164 cycles at 55°C every 22 seconds, which included the time to image the tubes. The reaction products were stored at -20°C for further analysis. The same procedure was used for second phase experiments, which lacked nickase and templates in the presence of approximately 4 μM of trigger. Precise trigger and dimer concentrations used when fitting the mathematical model were calculated by Nanodrop 2000c spectrophotometer measurements using extinction coefficients provided by the manufacturer, as the oligonucleotide concentrations provided by the manufacturer were approximated by a general extinction coefficient.

2.6 Urea denaturing polyacrylamide gel electrophoresis (PAGE) analysis

40% Acrylamide/Bis Solution, 29:1, Urea, 10× TBE buffer, 30% APS solution in water, TEMED, and MilliQ water were mixed to achieve final concentrations of 20% Acrylamide/Bis Solution, 29:1, 8M Urea, 0.5×TBE Buffer, 0.12% APS, and 0.05% (v/v) TEMED. The mixture was used to cast 0.75 or 1.00 mm gels with 15-wells using Mini-PROTEAN® Tetra Cell Casting Module, according to the manufacturer's protocol. The gels were pre-run for an hour in 0.5× TBE running buffer. Before loading the samples, the running buffer was heated to 60°C to ensure full denaturation of the UDAR products and secondary structures. The wells were flushed using a micro-pipettor for an even distribution of the sample on well surface. Samples were diluted as necessary in nuclease-free water, then diluted in sample running buffer (1μL sample, 2μL 1×TE buffer, 3μL Novex TBE-Urea sample buffer). Prepared samples were incubated at 70°C for 3 minutes and immediately placed on ice until loaded in the gel. Each gel included a 1 ng·μL^{-1} 10/60 Ladder and four concentration standards. Gels were run at 180 V for approximately 30 minutes in Bio-Rad Mini-PROTEAN® Tetra cell vertical mini gel electrophoresis. After staining with SYBR Gold solution (1×SYBR Gold, 0.5×TBE Buffer) for 9 minutes, gels were imaged by Invitrogen E-Gel® Imaging system with a Blue Light Base. The bands were quantified using GelAnalyzer 19.1 software (www.gelanalyzer.com) by Istvan Lazar Jr., PhD and Istvan Lazar Sr., PhD, CSc. The minimum peak height was set at 1.5 and rolling-ball background correction was set at 10% peak width tolerance. Concentrations were calculated using the quantity calibration curve derived from the concentration standards for each type of reaction product. Example calibration curves are provided in Fig. SI 1.

3 Results

3.1 Experimental product quantification produces proposed UDAR reaction mechanisms

UDAR is a novel DNA amplification reaction with unique biphasic output. The first phase of UDAR ends at a plateau, resembling an EXPAR reaction. After this plateau, the reaction enters a second phase, marked by a rapid increase in fluorescence output. This second phase signal creates a biphasic output (Fig. 1A and Figure SI 2), which to our knowledge had not been reported in literature for a DNA amplification reaction without addition of competitive agents, such as product sequestering templates or ex-

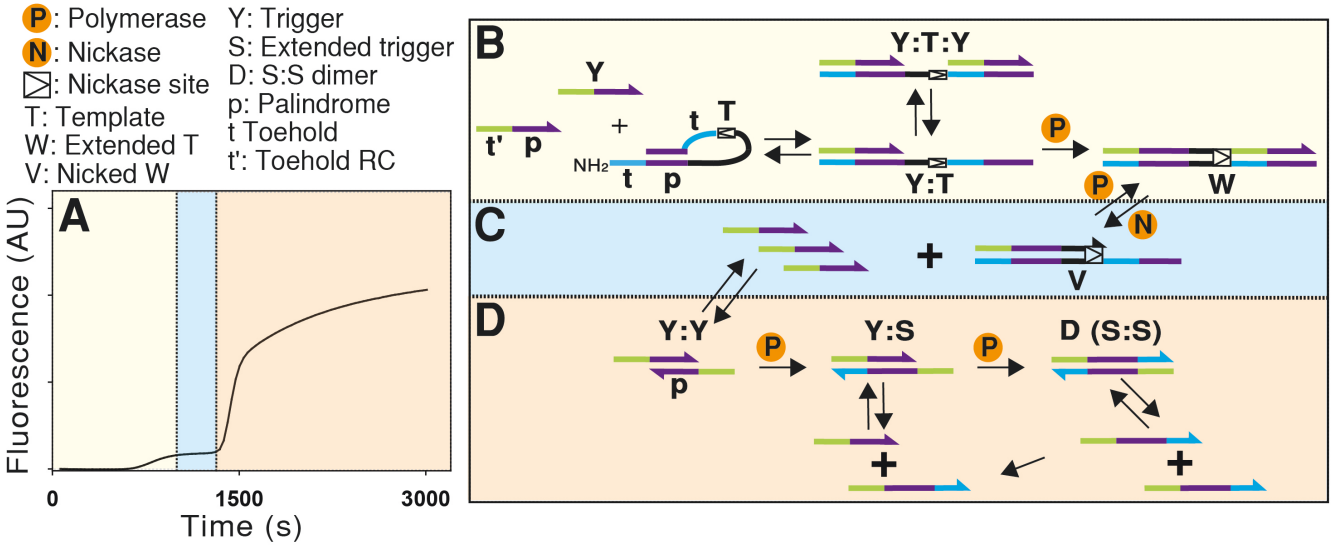

Fig. 1 UDAR reaction scheme. A) Fluorescence-time trace of the UDAR template, LS2. The shading shows the dominant reaction mechanisms responsible for each phase. B) First phase reaction pathways. The palindrome (p, shown in purple) causes the template (T) to fold into a looped configuration, as there are two trigger (Y) binding sites on the template (T). The reverse complement of the toehold on the trigger (t') can bind the toehold on the template (t) and unwind the palindrome to initiate amplification. C) Trigger production during the first phase and first plateau. Cyclical nicking and polymerization continuously produces trigger (Y). D) Second phase reaction pathways. The palindrome allows Y to weakly dimerize and enter the second phase. The looped configuration of S is not shown for simplicity, and extendable 3' ends of DNA are shown as arrows.

onucleases[30,31]. The unique properties of UDAR emerge from reaction pathways created by palindromic sequences (p) present in the template (T) and the triggers (Y), which are shown in purple in Fig. 1B-D. Quantitative PAGE-Urea analysis of UDAR products, collected at different time points throughout the reaction, revealed the presence of two distinct reaction products (Fig. 2), where the first phase produces triggers (Y) that become source materials for the second phase reaction products, dimers (D) and dimer monomers (S).

The data shown in Fig. 2 was used to associate a dominant UDAR reaction mechanism with each reaction phase (Fig. 1B-D). Similar to an EXPAR template, a UDAR template consists of a complementary sequence of a nicking endonuclease between two trigger binding sites. The reaction begins with the binding of an oligonucleotide trigger molecule to the template. These trigger molecules (Y) and synthetic reaction templates (T) contain palindromic regions (p), leading to the looped configuration of the template. The trigger can open the template by binding the toehold region (t:t' in Fig. 1) and displacing the palindromic stem (p) with the palindrome on the 3' end of the trigger. The open conformation of the template occurs during trigger binding, and is likely stabilized upon hybridization of two trigger molecules. Amplification initiates through the extension of a trigger molecule by the polymerase. This template extension creates a nicking endonuclease recognition site, allowing the nicking endonuclease to nick the top strand and free a newly created trigger. These triggers prime new templates, creating an initial increase in the fluorescence as the templates become double-stranded (Fig. 1B). The extended templates remain stably bound to their top strands, in both nicked (V) and unnicked (W) versions throughout the reaction. Thus, trigger production continues approximately linearly once the first phase ends (Fig. 1C), which can be seen for three different templates in the graph of product output (right axes) in Fig. 2D-F. We found that SYBR Green II is unable to stain triggers efficiently at the reaction conditions (Fig. SI 3), creating a plateau in the fluorescence output (Fig. 2D-F left axes, Fig. SI 2). The PAGE analysis is also shown in Fig. 2D-F, with the only product being the trigger Y and the double stranded templates W and presumably V. It is worth noting that the intermediate product V does not produce an easily visible band in the gel during the first phase.

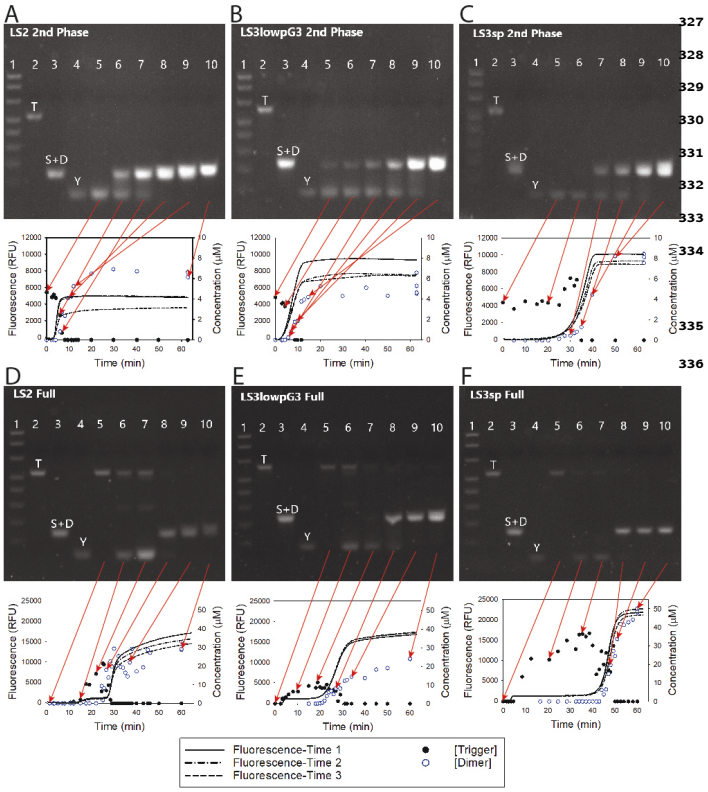

Fig. 2 Denaturing PAGE-Urea gels showing the products of each reaction corresponding to the fluorescence output of three different UDAR templates: LS2, LS3lowpG3, and LS3sp. Sequences can be found in Table SI 1. The first four lanes in all gels are 1) 1 ng·μL^{-1} 10/60 Ladder, 2) 0.2 μM template (T), 3) 1 μM dimer ($S+D$), and 4) 2 μM trigger (Y), with the exception of the LS3sp gels which have 5 μM Y standards. All second phase samples are undiluted. A) LS2 second phase reaction. B) LS3lowpG3 second phase reaction. C) LS3sp second phase reaction. D) LS2 full reaction, with samples in lanes 8-10 diluted 1:10. E) LS3lowpG3 full reaction, with samples in lanes 7-8 diluted 1:5 and lanes 9-10 diluted 1:10. F) LS3sp full reaction, with samples in lanes 7-8 diluted 1:5, lane 9 diluted 1:30, and lane 10 diluted 1:50.

The second phase is caused by an autocatalytic burst of secondary products D and S. As the triggers accumulate, extendable trigger:trigger hybrids are formed through hybridization of their palindromes (p) as shown in Fig. 1D. This association is weak, such that most triggers remain single stranded according to analysis by NUPACK. Trigger hybrids are extended by the polymerase, forming dimers D of the extended triggers. At the reaction conditions, extended trigger dimers can exist in both a single (S) and double stranded (D) form, with the monomer form (S) able to bind triggers (Y) with a higher stability than trigger:trigger binding. Polymerase converts trigger in the $Y:S$ complex to dimers. This scavenging of the trigger Y by the monomer S leads to a rapid autocatalytic increase in dimer (S or D) concentration and a concomitant decrease in the trigger (Y) concentration, which that can be seen in the PAGE analysis (Fig. 2D-F). Templates do not appear in the gel during the second phase of full reactions due to the necessary dilution of the reaction products. Reactions that isolate the second phase by initiation with trigger molecules and without templates or nickase also show the delayed switch between trigger and dimer products (Fig. 2A-C), similar to the second phase in the full UDAR reaction. Dimer production can be traced by fluorescence output as SYBR Green II efficiently stains the double-stranded dimers at the reaction conditions (Fig. SI 3). It is worth noting that S can additionally take on a looped form, as the 5' and 3' ends are self-complementary, which was seen when calculating DNA dissociation constants in NUPACK. The looped form of S was not included in the model as a separate product, however.

3.2 Mathematical Modeling

3.2.1 Full Reaction Model

The experimental data guided the mathematical model, which was built on mass action and enzyme kinetics. We model the UDAR reaction mechanisms using the following system of ODE's, which describe association, dissociation, elongation, and nicking events.

$$[\dot{Y}] = k_+(-2[Y]^2 + 2r_1[YY] - [Y][S] + r_2[YS]) + k_2[N][W]...$$

$$... - k_1[T](a_1[Y]^2 + a_2[Y])$$

$$[\dot{YY}] = k_+([Y]^2 - r_1[YY]) - \frac{k_{cat}}{L_{Y\to S}}P_0\frac{[YY]}{\kappa_1 C}$$

$$[\dot{YS}] = k_+([Y][S] - r_2[YS]) + \frac{k_{cat}}{L_{Y\to S}}P_0\frac{[YY]}{\kappa_1 C} - \frac{k_{cat}}{L_{Y\to S}}P_0\frac{[YS]}{\kappa_2 C}$$

$$[\dot{S}] = k_+(r_2[YS] - [Y][S] - 2[S]^2 + 2r_3[D])$$

$$[\dot{D}] = k_+([S]^2 - r_3[D]) + \frac{k_{cat}}{L_{Y\to S}}P_0\frac{[YS]}{\kappa_2 C}$$

$$[\dot{W}] = k_1[T](a_1[Y]^2 + a_2[Y]) - k_2[N][W] + \frac{k_{cat}}{L_{V\to W}}P_0\frac{[V]}{\kappa_3 C}$$

$$[\dot{V}] = k_2[N][W] - \frac{k_{cat}}{L_{V\to W}}P_0\frac{[V]}{\kappa_3 C}$$

$$[\dot{N}] = -\beta[N]$$

where

$$C = 1 + \frac{[YY]}{\kappa_1} + \frac{[YS]}{\kappa_2} + \frac{[V]}{\kappa_3} + \frac{[W]}{\kappa_4}$$

$$[T] = T_0 - [W] - [V]$$

The first phase of UDAR is dependent on converting the template (T) to the double stranded template W through the binding and extension of trigger Y (see Fig. 1). The trigger molecule (Y) binds to a template molecule (T) with the association rate k_+ and a dissociation rate a_1k_+ and a_2k_+ for two triggers binding to a single template or one trigger bound to a template, respectively. The parameters a_1 and a_2 are equilibrium association constants; the initial association of trigger and template are assumed to equilibrate quickly due to the excess of template molecules. The parameter k_1 describes elongation of the trigger-bound template into the double stranded template W. W then enters an amplification cycle where it is continuously nicked by nickase N at the

rate k_2 to produce a trigger Y, leaving a nicked template V. The elongation of V to W by the polymerase is described by Michaelis-Menten kinetics, where the Michaelis-Menten constant is κ_3 and the catalytic constant is $\frac{k_{cat}}{L_{V\to W}}$, where $L_{V\to W}$ is the length of the extended section in nucleotides. As template is not produced in the reaction, the number of template strands is conserved. Therefore the initial template concentration T_0 is distributed between the species T, W, and V at all times. The parameter C found in the denominator of the Michaelis-Menten term is acknowledging the competition between DNA species YY, YS, V and W for polymerase. Nickase (N) gradually loses activity over time with the rate β. The produced Y inefficiently dimerizes through hybridization of the palindrome p and enters the second phase reaction as described in 3.2.2.

3.2.2 Second Phase Reaction Model

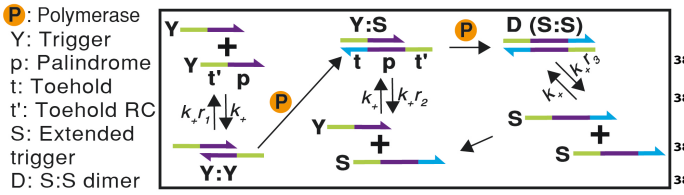

Fig. 3 Reaction scheme describing the isolated second phase of UDAR. The trigger (Y) can weakly dimerize due to the presence of the palindrome (p) on their 3' end. The polymerase can extend this into an extended trigger (S), which can bind triggers with more stability than trigger dimerization and therefore can scavenge free triggers to create more S. S exists both in single stranded (S) and double stranded (D) configurations. The looped form of S is not shown for simplicity, and the model association and dissociation constants are shown.

We experimentally and mathematically isolated the second phase of UDAR to determine the parameters associated with the secondary burst in reaction products. The second phase of UDAR can be reproduced by fitting the following simplified ODE system of equations.

$$[\dot{Y}] = -2k_+[Y]^2 + 2k_+r_1[YY] - k_+[Y][S] + k_+r_2[YS]$$

$$[\dot{YY}] = k_+[Y]^2 - k_+r_1[YY] - \frac{k_{cat}}{L_{Y\to S}}P_0\frac{[YY]}{\kappa_1 C}$$

$$[\dot{YS}] = k_+[Y][S] - k_+r_2[YS] + \frac{k_{cat}}{L_{Y\to S}}P_0\frac{[YY]}{\kappa_1 C} - \frac{k_{cat}}{L_{Y\to S}}P_0\frac{[YS]}{\kappa_2 C}$$

$$[\dot{S}] = k_+r_2[YS] - k_+[Y][S] - 2k_+[S]^2 + 2k_+r_3[D]$$

$$[\dot{D}] = k_+[S]^2 - k_+r_3[D] + \frac{k_{cat}}{L_{Y\to S}}P_0\frac{[YS]}{\kappa_2 C}$$

$$C = 1 + \frac{[YY]}{\kappa_1} + \frac{[YS]}{\kappa_2}.$$

The second phase of UDAR is dependent on converting the trigger (Y) into an extended trigger, called S in its single stranded form and D in its double stranded form (Fig. 3). Y can weakly dimerize through hybridization of the palindromic region p with association rate k_+ and dissociation rate r_1k_+. This complex can be extended to become a dimer (D) with Michaelis-Menten constant κ_1 and catalytic constant $\frac{k_{cat}}{L_{Y\to S}}$, where $L_{Y\to S}$ is the length of the extended section in nucleotides. D can dissociate into two single stranded molecules, S, with association rate of k_+ and dissociation rate r_3k_+. The single stranded (S) can scavenge triggers (Y) with association rate k_+ and dissociation rate r_2k_+, and species YS can create dimer (D) through polymerase with Michaelis-Menten constant κ_2 and catalytic constant $\frac{k_{cat}}{L_{Y\to S}}$. The DNA dissociation constants of YY, YS, and D are r_1, r_2, and r_3, respectively. The parameter C found in the denominator of the Michaelis-Menten term is acknowledging the competition between DNA species YY and YS for polymerase. Trigger is not produced without template, such that the initial starting concentration of trigger molecule (Y) is converted to S and D by dimerization and extension by polymerase.

3.3 Model parameters

3.3.1 Selection of model parameters

Model parameters were determined by literature, manufacturer information, and online resources; a full list of the final parameters is found in Table 1. The dissociation constants r_1, r_2, r_3 and association constants a_1 and a_2 of YY, YS, D (SS), Y^2T, and YT respectively, were estimated from NUPACK[22]. The settings were as follows: nucleic acid type was DNA, Na^+:= 0.06 M, Mg^{++}:= 0.006 M, temperature = 55°C, and dangle treatment set to "Some". The order of magnitude of the DNA:DNA association rate for 10 nt long oligonucleotides, k_+, was calculated at the UDAR reaction temperature using the Arrhenius plot prepared by Morrison et al.[33], based on their experiments where their test conditions had much higher ionic strength compared to UDAR. The rate k_+ was used as the general association rate for all oligonucleotides in the model, justified by the small change in the association rate for oligonucleotides of different sizes; for example, the association constant for 10 nt oligonucleotides is half that of 20 nt oligonucleotides. In contrast, the dissociation rate changed by over five orders of magnitude. The dissociation rates were therefore determined by multiplying the general association rate by the dissociation constant determined by NUPACK. A further analysis of the sensitivity of the model on the association rate was performed below.

The Michelis-Menten constants for YY extension (κ_1), YS extension (κ_2), V extension (κ_3) and W-polymerase interaction (κ_4) were included in the model. The parameters κ_1 and κ_2 were obtained from the numerical fit of the second phase data for each template, while κ_3 was obtained by fitting the full UDAR model. The parameter κ_4 is used in the competition term C, and acknowledges the ability of Bst polymerase to bind double stranded DNA as it has A-tailing capabilities (NEB customer support). κ_4 was assumed to be approximately equal to κ_3; this assumption was analyzed in further detail below. The rate of nucleotide incorporation, k_{cat}, was obtained from NEB customer support, where it was determined for the same enzyme operating in loop-mediated amplification reaction (LAMP) conditions, at 65°C. Nicking en-

Table 1 Model parameters

Parameter	Definition	Source	LS2	LS3lowpG3	LS3sp	Unit
k_+	Association Rate, DNA-DNA hybridization	Morrison et. al.[32]	1.00×10^{1}	1.00×10^{1}	1.00×10^{1}	$s^{-1}\mu M^{-1}$
r_1	$Y:Y$ dissociation constant	NUPACK	1.2×10^{3}	1.4×10^{3}	1.5×10^{4}	μM
r_2	$Y:S$ dissociation constant	NUPACK	3.7×10^{1}	1.8×10^{1}	1.6×10^{1}	μM
r_3	$S:S$ dissociation constant	NUPACK	4.7×10^{0}	8.8×10^{-1}	7.2×10^{-2}	μM
a_1	$2Y:T$ association constant	NUPACK	2.0×10^{-4}	9.0×10^{-2}	4.0×10^{-2}	μM^{-2}
a_2	$Y:T$ association constant	NUPACK	1.4×10^{-2}	3.9×10^{-1}	2.0×10^{-1}	μM^{-1}
κ_1	MM constant, $Y:Y$ extension	second phase fit	1.0×10^{4}	1.0×10^{4}	1.0×10^{6}	μM
κ_2	MM constant, $Y:S$ extension	second phase fit	3.5×10^{-1}	3.5×10^{-1}	8.9×10^{-1}	μM
κ_3	MM constant, V extension	full reaction fit	2.6×10^{-2}	5.8×10^{-2}	3.6×10^{-2}	μM
κ_4	MM constant, W sequestration	assumed to be $=\kappa_3$	2.6×10^{-2}	5.8×10^{-2}	3.6×10^{-2}	μM
k_{cat}	Nucleotide incorporation rate	NEB customer support	1.0×10^{2}	1.0×10^{2}	1.0×10^{2}	$nt\cdot s^{-1}$
k_1	Polymerization rate, $Y:T$ extension	full reaction fit	7.6×10^{-1}	5.2×10^{-2}	2.6×10^{-1}	s^{-1}
k_2	Nicking rate	full reaction fit	2.6×10^{1}	2.6×10^{1}	2.6×10^{1}	$s^{-1}\mu M^{-1}$
β	Nickase deactivation rate	nickase deactivation fit	6.0×10^{-4}	6.0×10^{-4}	6.0×10^{-4}	s^{-1}
n_0	Nickase Initial Concentration	Estimated from manufacturer	2.6×10^{-2}	2.6×10^{-2}	2.6×10^{-2}	μM
p_0	Polymerase Initial Concentration	Estimated from manufacturer	5.0×10^{-3}	5.0×10^{-3}	5.0×10^{-3}	μM

donuclease deactivation rate, β, was investigated experimentally and discussed in greater detail below.

3.3.2 Optimization of model parameters fit to experimental data

A MATLAB minimization algorithm, fmincon, was used to optimize the values of several parameters; the constraints used are given in Table SI 2. The function being minimized was

$$\sum_{j=1}^{m}\sum_{i=1}^{n_j}(w_i(Y_j(t_i)-\widehat{Y}(t_i))^2+w_i(S_j(t_i)-\widehat{S}(t_i))^2)$$

where w_i is the weight associated with data point i, m is the number of data sets being fit for a particular template, n_j is the number of time points measured in data set j. The first term compares the observed amount of trigger at time t_i in the experimental data set j, $Y_j(t_i)$, and the predicted total amount of trigger at time t_i from the model, $\widehat{Y}(t_i)$, calculated by $[Y]+2[YY]+[YS]$. The second term compares the observed amount of extended trigger at time t_i in data set j, $S(t_i)$, and the predicted amount of extended trigger from the model at time t_i, $\widehat{S}(t_i)$, calculated by $[S]+2[D]+[YS]$.

The first parameters that were optimized were κ_1 and κ_2, with all other parameters determined from NUPACK (see Table 1). This was achieved by fitting the second-phase data, with the results of this fit found in section 3.4. In the next phase of the fitting procedure, we used the optimized κ_1 and κ_2 values to fit the remaining parameters k_1, k_2, and κ_3 to the full reaction data; the results of this fit can be found in section 3.5. In this process we assumed that $\kappa_4=\kappa_3$; we investigated the effect of this assumption in the sensitivity analysis below.

3.3.3 Analysis of polymerase activity

Bst 2.0 WarmStart® DNA Polymerase is a popular polymerase for many isothermal DNA amplification chemistries with strong strand displacement capabilities and thermostability. However, according to the manufacturer's technical information page, Bst 2.0 WarmStart® DNA Polymerase leaves 3' A overhangs, which would hinder dimer production of UDAR. A-tailed trigger extension would be inhibited as $Y:Y$ hybrids would have 3' overhangs, disrupting trigger extension. In order to assess if A-tailed triggers significantly contributed to the second phase signal, second phase experiments were conducted with A-tailed versions of the triggers, along with non-modified triggers as control samples and non-modified triggers without polymerase as background fluorescence control samples (Fig. SI 4). The A-tailed triggers did not replicate the second phase kinetics while the non-modified triggers were converted into highly fluorescent dimers. All visible trigger molecules on the gel appeared to convert to dimers during the second phase (Figure 2), implying that triggers were infrequently A-tailed by Bst polymerase during UDAR reactions. This was consistent with previous observations; the nucleotide after the trigger binding site of EXPAR templates were chosen to be T, to compensate for A-tailing activity of the polymerase although evidence for this activity was not observed[34]. Given the lack of evidence for a high concentration of A-tailed products, polymerase A-tailing was not included in the mathematical model.

The parameter κ_4 was included in the model to acknowledge that Bst polymerase can rebind to double stranded DNA (personal communication, NEB). The hypothesized polymerase binding to fully double stranded DNA occurs for the purpose of A-tailing, although our experiments did not show evidence of a large concentration of products with an additional A on the 3' end. We therefore investigated the effect of excluding the κ_4 term from the polymerase competition parameter C. We additionally investigated including competition from the double stranded dimer D in addition to the double stranded templates V and W. Without κ_4, the model still reproduced the rise and fall of Y, as well as the steep second phase rise dimer D and monomer S (Fig. SI 5A). However, the error of the fit increased without the inclusion of κ_4 (Table SI 3), so the parameter κ_4 was included in the final model. The inclusion of this W competition does not confirm that polymerase is binding to the double stranded template. While it is possible that polymerase is binding to the template but does not frequently add an additional A nucleotide, it is also possible that the improved fit is due to a small error in the calculated ratio between W and V or from other unknown errors in model parameters. Including competition from D in the second phase fit decreased the rate of second phase growth (Fig. SI 5B) and increased the model error (Table SI 3), presumably from the rapid

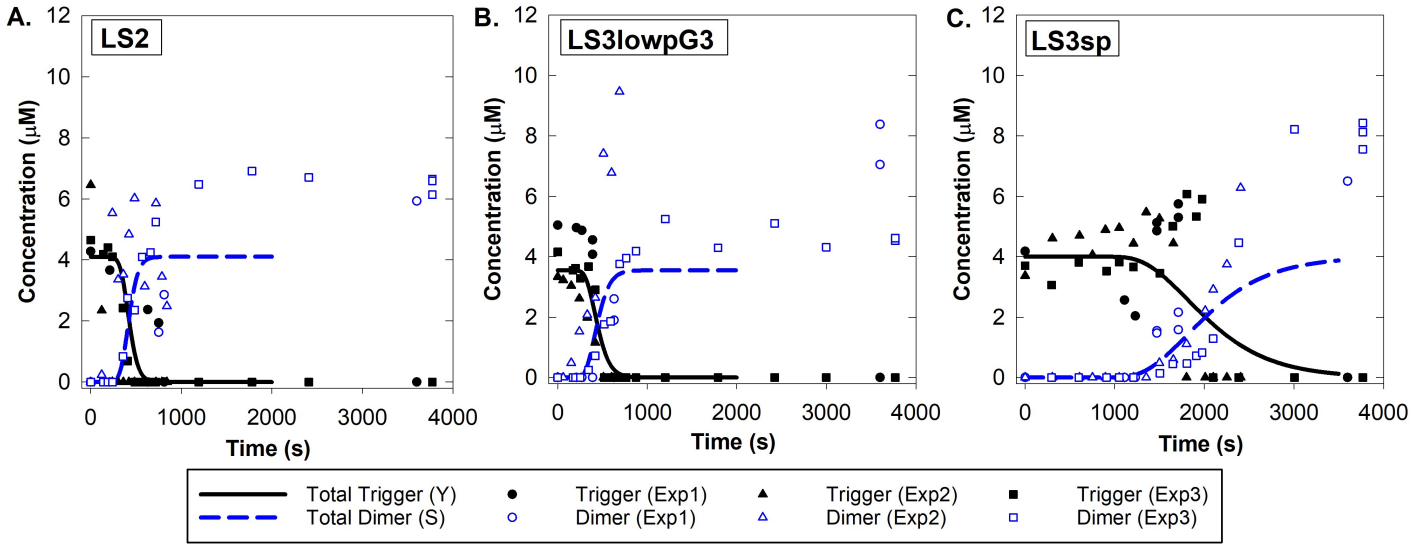

Fig. 4 Second phase fits with the simulated total trigger (Y) shown as solid black lines and total dimer (all forms of S, total dimer $= S+2D+YS$) shown as dashed blue lines for each template. The raw data points show three independent experiments. A) LS2 template B) LS3lowpG3 template C) LS3sp template

rise of dimer products during the second phase leading to significant polymerase competition. Competition from polymerase re-binding to D was therefore not included in the final model. While it is possible that the parameter κ_4 does not need to be included in the model, the effect of including this term on the fit parameters was modest (Table SI 4).

Additionally, Bst 2.0 WarmStart® DNA Polymerase was tested for possible activity loss with incubation at the reaction conditions. For this purpose, EXPAR was used as it has similar reaction conditions as UDAR but with simpler reaction mechanisms. Bst 2.0 WarmStart® DNA Polymerase was incubated in EXPAR reaction mix that did not contain nicking endonuclease and template, at 55°C for 0, 10, 20, 30, 40, 50 and 60 minutes. When the nicking endonuclease and template were added to the mix, 55°C incubation continued and real-time fluorescence imaging was conducted. No change in reaction output was observed for samples with pre-incubated polymerase (Fig. SI 6). We therefore did not include polymerase deactivation in the model.

3.3.4 Analyzing nicking endonuclease activity

Previous reports showed that nickase slowly deactivates over time during EXPAR reaction conditions[11]. To quantify this effect for use in the mathematical model, we used EXPAR in a manner similar to the polymerase deactivation experiments cited above. Briefly, nicking endonuclease was pre-incubated in a reaction mix that did not contain polymerase and template at 55°C for 0, 10, 20, 30, 50 and 60 minutes. When polymerase and an EXPAR template were added to the mix, 55°C incubation continued and real-time fluorescence imaging was conducted. A significant decrease in the overall reaction rate was observed with increased 55°C incubation times (Fig. SI 7A). This data was used to estimate the decay of the nickase activity over time, which is represented by the parameter β in our model. We made several simplifying assumptions during the calculation of this parameter. In addition, UDAR reaction mix contained 6.08% glycerol, which is not included in the EXPAR reactions. The overall reaction rate was assumed to be proportional to the nicking rate, and the reaction was assumed to be a saturating exponential function. The overall reaction rate for each pre-incubation time was calculated assuming the inflection points occurred at approximately half the maximum fluorescence values. With these assumptions, the overall reaction rate exponentially decreased at a rate of β (Fig. SI 7B). Given the number of assumptions made during this calculation and possible differences between UDAR and EXPAR, these assumptions were tested by fitting the parameter β to an ordinary differential equation model of EXPAR using model parameters found in the full UDAR fit. This model showed good agreement with the experimental inflection points with a β of 0.000757, which differed from our original estimate by 26% (Fig. SI 7C). This change in β had a minimal impact on the model output (Fig. SI 7D); the original value of $\beta = 0.0006$ was therefore maintained for the full reaction fit. Details of these calculations are given in the ESI.

3.4 Reproducing second phase kinetics with a mathematical model

The second phase was reproduced by mixing trigger and polymerase in UDAR reaction buffer that did not contain nickase and template, and the resulting trigger and dimer concentrations were measured over time using quantitative PAGE. Without template, the reaction was unable to produce new trigger. We therefore achieved isolation of the reaction that converted the initial trigger Y to dimers S and D. All reactions contained weaker YY binding when compared to YS binding as seen by the approximately $2-3$ order of magnitude difference between r_1 and r_2; the initial formation of S from $Y:Y$ was slow, but scavenging of Y by S was much more favorable. The governing equations are provided in section 3.2.2. The parameters κ_1 and κ_2 were fit using this data, and can be found in Table 1.

The timing of the trigger-to-dimer exchange varied within each template, so the data were adjusted to the mean start time for each template before optimization was performed. This adjustment assured that the slopes of the dimer rise and trigger fall were not lost while the approximate rise time of dimer was maintained. The start time for each data set defined as the time when the first measurable dimer concentration ($\geq 0.3\mu M$) was achieved, which was determined by linearly interpolating between data points. The the start times for the second-phase experiments for LS2, LS3lowpG3, and LS3sp were 360 ± 272 s, 303 ± 163 s, and 1437 ± 150 s, respectively. The weights and corresponding time intervals for this optimization are listed in Table 2. The numerical fit of the data is shown over the raw data in Fig. 4.

The templates used in this study were related, but with key differences between the palindrome and toehold sequences, which changed the stability of DNA binding. LS3lowpg3 had the same palindrome as LS2, but a longer toehold region. The initial formation of trigger dimers YY and subsequent conversion to YS should therefore be very similar, which was seen in the nearly identical fit parameter κ_1 between the two templates. The similar 3' end between LS2 and LS3lowpg3 triggers (Y) may possibly also have led to the similar fit κ_2 between the two templates. The double stranded dimer D and folded monomer S were more stable, however, which left fewer single stranded S strands to scavenge the trigger Y. The increased stability of dimer D could be seen by a decrease in the dissociation constant r_3. This may explain why the rise was not as sharp for LS3lowpG3 when compared to LS2 (Fig. 2). LS3sp had a shorter, GC-rich palindrome when compared to the other two templates, but the same toehold as LS3lowpG3. The large κ_1 found for LS3sp suggests that polymerase elongation of a 4 nucleotide double stranded region was highly unfavorable at our reaction conditions. The combination of stable secondary structures of S and D strands due to the long GC stretch also appeared to contribute to a later second phase rise. The fit for this template reproduced the delayed second phase dimer rise, but did not reproduce the sharp rise seen in the data. This template showed the limitations of the model to reproduce the most extreme UDAR template product output.

3.5 Reproducing full reaction output with a mathematical model

Using the full system of equations, as defined in section 3.5, the k_1, k_2, and κ_3 were fit to the product output of trigger and dimer from the full reaction data. The nicking rate k_2 was constant across templates, so the model was fit to individual templates and the mean k_2 value was calculated across all templates. Using this mean k_2, the values of k_1 and κ_3 were re-optimized for each template separately using the full reaction data. Table 2 gives weights and time intervals. The fit of the full reaction output yielded parameters given in Table 1. Figure 5 shows that the numerical reaction output can reproduce the approximate production time of trigger and dimer, although the numerical model for LS3sp did not reproduce the sharp dimer rise seen experimentally. This template had the shortest palindrome at 4 nucleotides, making initial production of the dimer S unfavorable and the associated reaction parameters κ_1 and r_1 large. LS3sp again appeared to approach the limit of what the model could reproduce.

The time series data shown here was challenging to fit, as the product output changed rapidly during short time intervals followed by long time intervals of slow product change. The regular L_2 norm weighed error between the data and the numerical simulation equally for each time point, while often the goodness of fit is judged by the model's ability to fit a particular feature of the data. We used different weights for fitting different aspects of the UDAR output, as detailed in Table 2. In particular, when fitting second phase data, we concentrated on fitting the transition which fell between indicated times in column 1. Other time points had weight 0 and therefore did not enter the goodness of fit cost function. Similarly, for full model fit the error during the initial time interval that contained both first and second rise was weighted more than the last portion of the data that appeared to contain more experimental variability.

Table 2 Minimization Weights and Average Cut-off Times, in Seconds: During the fitting process, data points associated with a time less than the first listed value received the first weight, times between the two listed values received the second weight, and values greater than the second listed value received the third weight. During the second phase fit for parameters κ_1 and κ_2, the average cut-off time was used. The fit to the full reaction for k_1, k_2, and κ_3 used cut-off times found for each experimental data set, with the average cut-off times reported here.

	Second-Phase	Full	Refitted Full
weight	0, 1, 0	10, 1, 1	20, 1, 1
LS2	360, 500	1540, 1897	1540, 1897
LS3lowpG3	303, 540	1183, 1980	1183, 1980
LS3sp	1437, 2470	2513, 3080	2513, 3080

3.6 Sensitivity Analysis

We made several assumptions when determining model parameters. To analyze the effect of these assumptions on the quality of the fit we performed a sensitivity analysis on the model parameters k_+, κ_4, κ_3, and k_{cat}.

The overall DNA association rate k_+ was calculated from literature as described above. As changes in the DNA association rate are small when compared to DNA dissociation rates when varying nucleotide length and temperature, we used a general DNA association rate in the model that is the same order of magnitude as a 10nt DNA strand associating at the UDAR reaction temperature [33]. Sensitivity analysis on the DNA association rate, k_+, was performed using the numerical model for the template LS2. Figure 6 shows that the model is not sensitive to k_+, with a minimal impact on the model with an order of magnitude increase or decrease in the parameter (Figure 6A). This shows that using a DNA association constant within the correct order of magnitude should minimally affect the overall model.

The parameters κ_4 and κ_3 were assumed to be equal because both V and W are long, double stranded DNA molecules. The fit was modestly affected when optimization was performed assuming that κ_4 differs from κ_3 by one order of magnitude (Figure 6B). A larger κ_4 made the predicted dimer rise to initiate slightly earlier, but maintained the features of the UDAR reaction. Therefore

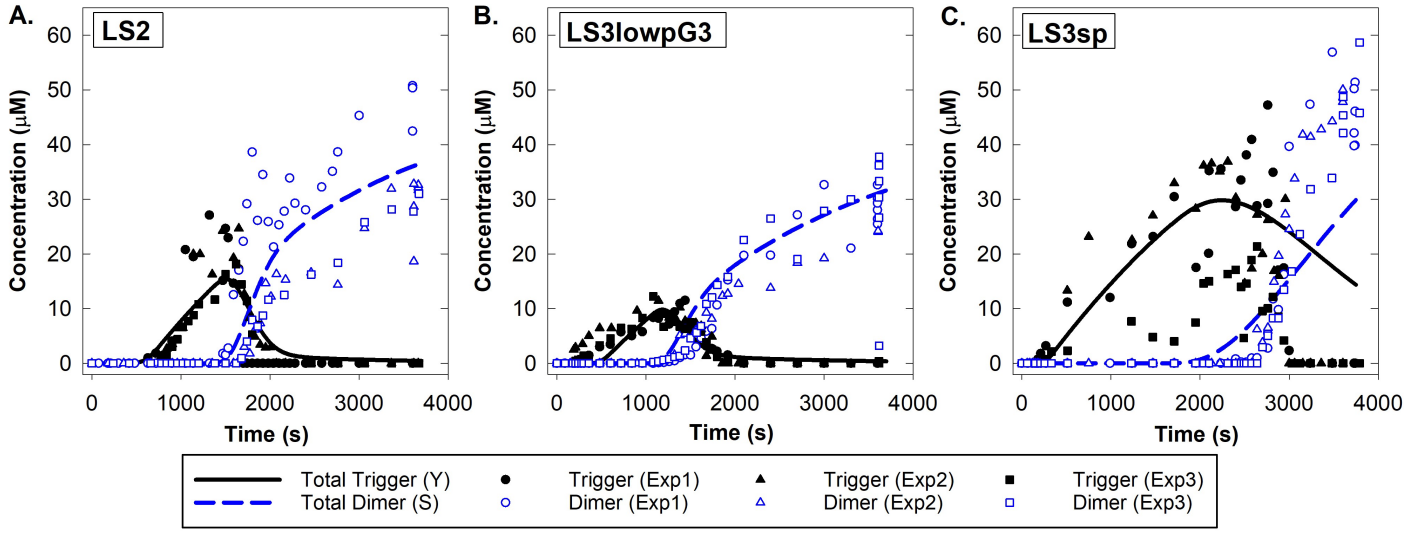

Fig. 5 Full experiment fits with the simulated total trigger (Y) shown as solid black lines and total dimer (all forms of S, total dimer $= S+2D+YS$) shown as dashed blue lines for each template. The raw data points show three independent experiments. A) LS2 template B) LS3lowpG3 template C) LS3sp template

the model can still reproduce the sharp second rise that is characteristic of UDAR reactions for a range of values for κ_4.

The polymerization rate k_{cat} was also determined without experimental confirmation. The actual value of k_{cat} was likely smaller than the manufacturer's statement of 100/s as the manufacturer's measurement was at 65°C, while the UDAR reaction occured at 55°C and contained different salt concentrations. To address the potentially slower polymerization rate due to the lower reaction temperature and modified solution conditions, the model was fit using a k_{cat} of $50s^{-1}$ - $100s^{-1}$. The optimal model output is again slightly modified, with the major features of UDAR reproduced (Figure 6C).

Nucleic acid stains such as SYBR™ Green II have previously been shown to modify DNA dissociation constants. SYBR™ Green II was included in the reaction mix to monitor kinetics. If the dissociation constants r_1, r_2, and r_3 are increased or decreased by 50% during the fitting process, then the second phase fits were very slightly shifted to the left or right, respectively (Figure 6D). The difference between DNA dissociation constants between different species in this study ranged over five orders of magnitude. The assumed change in dissociation constants from changing solution conditions analyzed here did not have a large impact on the optimal model output.

A summary of the fit parameters produced when varying the values of k_+, κ_4, κ_3, and k_{cat} is given in Table 3. We conclude that the overall affect of varying the parameters was notable but small. The model assumptions may have affected the accuracy of the fit parameters, but did not appear to have affected the characteristic biphasic output reported here.

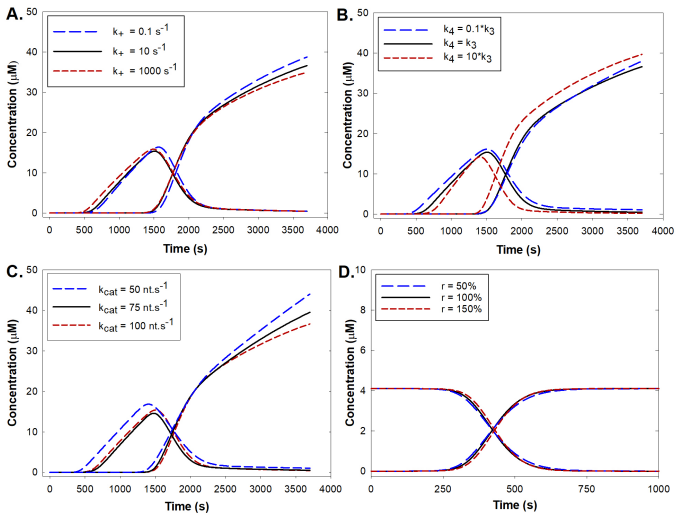

Fig. 6 Sensitivity analysis for the LS2 model. Optimization was rerun while varying several parameters to see the effect on the numerical model output. A) The effect of increasing and decreasing k_+ by one order of magnitude. B) The effect of changing κ_4 relative to κ_3. C) The effect on decreasing k_{cat} from the manufacturer's stated 100/s. D) The effect of increasing and decreasing r_1, r_2, and r_3 by 50%.

3.7 Limitations of the Model

While the computations can reproduce the biphasic behavior of the UDAR reaction output, it is important to acknowledge the limitations of the ODE model. Nonspecific amplification, which is a common issue in isothermal amplification reactions[34] was not included to simplify the model and focus on analyzing the mechanism and kinetics of the second phase signal burst. If nonspecific amplification was included, then the fit k_1 value would likely be modified as k_1 affects the timing of the initial trigger rise. As κ_3, k_2, and k_1 are fit together, simplifying the first phase reac-

Table 3 Sensitivity analysis for the LS2 model was performed for several parameters. The affect on the fit parameters k_1, k_2, κ_1, κ_2, and κ_3 are shown for each scenario. N/A indicates that this parameter was not refit and therefore the same as in the original fit.

	$\mathbf{k_1}$ (s^{-1})	$\mathbf{k_2}$ ($s^{-1}\mu M^{-1}$)	κ_1 (μM)	κ_2 (μM)	κ_3 (μM)
LS2 Original Fit	7.6E-01	2.6E+01	1.0E+04	3.50E-01	2.6E-02
$\mathbf{k_{cat} = 50}$ **(nt/s)**	6.9E-01	1.6E+02	8.5E+03	1.6E-01	2.2E-02
$\mathbf{k_{cat} = 75}$ **(nt/s)**	5.3E-01	4.4E+01	1.0E+04	2.5E-01	3.1E-02
$\kappa_4 = 0.1 * \kappa_3$ **(μM)**	8.0E-01	9.4E+01	N/A	N/A	4.7E-02
$\kappa_4 = 10 * \kappa_3$ **(μM)**	5.5E-01	2.1E+01	N/A	N/A	1.0E-02
0.5*r (μM)	N/A	N/A	9.9E+03	6.4E-01	N/A
1.5*r (μM)	N/A	N/A	1.0E+04	2.4E-01	N/A
$\mathbf{k_+ = 0.1}$ **($s^{-1}\mu M^{-1}$)**	5.7E-01	2.9E+01	9.8E+03	2.8E-01	2.1E-02
$\mathbf{k_+ = 1000}$ **($s^{-1}\mu M^{-1}$)**	1.1E+00	2.2E+01	9.9E+03	3.5E-01	2.2E-02

tion may decrease the absolute accuracy of the model parameters. While we addressed some potential sources of error by providing a sensitivity analysis of key model parameters, assumptions made for each parameter could compound to produce further error in the model parameters determined in this study. Changing solution conditions would also modify the model parameters. For example, the addition of glycerol to stabilize enzymes can potentially inhibit polymerase function and decrease product formation. Changing the concentration or type of fluorescent DNA dye would likely have a similar effect on the reaction, as some commonly used DNA binding dyes are known to inhibit DNA amplification [35]. Additionally, while multiple initial conditions were used to prevent the optimization software from becoming trapped in a local minimum, it is possible that a more optimal global minimum exists that the software did not find. The absolute accuracy of parameters that we have found should therefore be taken with caution, particularly when using reaction conditions that differ from those in this study.

4 Conclusions

UDAR is a novel, isothermal DNA amplification chemistry with unique, biphasic and switch-like kinetics. Quantitative PAGE was used to measure UDAR reaction products over time, which showed that the sharp second phase rise in fluorescence was due to the rapid, autocatalytic conversion of the first phase products, triggers, into extended dimers. A mathematical model built from proposed dominant reaction mechanisms reproduced the production and conversion of the trigger molecules for three different UDAR triggers, as well as the sharp rise in dimers that produced the second phase fluorescence. The model was limited by assumptions made during parameter selection, such as potential error in the dissociation rates due to the affect of SYBR Green II on DNA hybridization kinetics, uncertain nucleotide incorporation rate for specific UDAR conditions, assumptions on polymerase competition with double stranded DNA, an assumed universal DNA association rate, and exclusion of nonspecific amplification from the model. These limitations were addressed with sensitivity analysis and further simulations, which showed that the model could still reproduce the sharp second phase rise in extended dimers within the range of assumed parameter uncertainties. Absolute accuracy of the model parameters must be taken with caution, however, particularly when modifying experimental conditions.

UDAR provides a unique, non-linear, biphasic DNA amplification reaction with predictable product output. The second phase nonlinear burst of product is unique to UDAR, with a larger signal and a sharper signal rise than existing nucleic acid amplification techniques. These unique kinetics expand the toolbox of amplification reactions and could be used for definitive detection of a variety of molecules from RNA to proteins. The associated mathematical model opens possibilities of computational experiments, which could be used when designing reaction schemes to manipulate product output of UDAR. Further, the techniques seen here could guide computational modeling efforts for other isothermal nucleic acid amplification reactions.

Author Contributions

BO and EES collected experimental data, SDM created Matlab code and fit experimental data, SEM, SDM, and TG created the ODE model, all authors contributed to writing the publication.

Conflicts of interest

SEM and TG have a patent application pertaining to the reaction described in this work.

Acknowledgements

This material is based upon work supported by the National Science Foundation under Grant Number 1847245 and by the Office of the Assistant Secretary of Defense for Health Affairs, through the Peer Reviewed Medical Research Program, Discovery Award under Award No. W81XWH-17-1-0319.

Notes and references

1 E. A. Pumford, J. Lu, I. Spaczai, M. E. Prasetyo, E. M. Zheng, H. Zhang and D. T. Kamei, *Biosensors and Bioelectronics*, 2020, **170**, 112674.

2 S. Kumar, A. Kumar and G. Venkatesan, *Journal of Genetics and Genomes*, 2018, **2**, 1000112.

3 M. S. Reid, X. C. Le and H. Zhang, *Angewandte Chemie International Edition*, 2018, **57**, 11856–11866.

4 C. Qian, R. Wang, H. Wu, F. Ji and J. Wu, *Analytica Chimica Acta*, 2019, **1050**, 1–15.

5 Y. Mori and T. Notomi, *Journal of Infection and Chemotherapy*, 2020, **26**, 13–17.

6 N. V. Zyrina and V. N. Antipova, *Biochemistry*, 2021, **86**, 887–897.

7 B. Özay and S. E. McCalla, *Sensors and Actuators Reports*, 2021, **3**, 100033.

8 J. L. Gevertz, S. M. Dunn and C. M. Roth, *Biotechnology and Bioengineering*, 2005, **92**, 346–355.
9 M. W. Pfaffl, *Nucleic Acids Research*, 2001, **29**, e45–e45.
10 E. Rubin and A. A. Levy, *Nucleic Acids Research*, 1996, **24**, 3538–3545.
11 J. Van Ness, L. K. Van Ness and D. J. Galas, *Proceedings of the National Academy of Sciences*, 2003, **100**, 4504–4509.
12 J. Chen, X. Zhou, Y. Ma, X. Lin, Z. Dai and X. Zou, *Nucleic Acids Research*, 2016, **44**, e130–e130.
13 C. Moody, H. Newell and H. Viljoen, *Biochemical Engineering Journal*, 2016, **112**, 193–201.
14 Y. Kimura, M. J. L. de Hoon, S. Aoki, Y. Ishizu, Y. Kawai, Y. Kogo, C. O. Daub, A. Lezhava, E. Arner and Y. Hayashizaki, *Nucleic Acids Research*, 2011, **39**, e59–e59.
15 S. Subramanian and R. D. Gomez, *PLOS ONE*, 2014, **9**, 1–10.
16 L. Schneider, H. Blakely and A. Tripathi, *ELECTROPHORESIS*, 2019, **40**, 2706–2717.
17 N. Kaur, N. Thota and B. J. Toley, *Computational and Structural Biotechnology Journal*, 2020, **18**, 2336–2346.
18 K. Montagne, R. Plasson, Y. Sakai, T. Fujii and Y. Rondelez, *Molecular Systems Biology*, 2011, **7**, 466.
19 D. Y. Zhang, A. J. Turberfield, B. Yurke and E. Winfree, *Science*, 2007, **318**, 1121–1125.
20 B. Özay, C. M. Robertus, J. L. Negri and S. E. McCalla, *Analyst*, 2018, **143**, 1820–1828.
21 D. Ciesielski, B. Özay, S. McCalla and T. Gedeon, *Journal of The Royal Society Interface*, 2019, **16**, 20190143.
22 J. N. Zadeh, C. D. Steenberg, J. S. Bois, B. R. Wolfe, M. B. Pierce, A. R. Khan, R. M. Dirks and N. A. Pierce, *Journal of Computational Chemistry*, 2011, **32**, 170–173.
23 R. Nutiu and Y. Li, *Journal of the American Chemical Society*, 2003, **125**, 4771–4778.
24 Z.-z. Zhang and C.-y. Zhang, *Analytical chemistry*, 2012, **84**, 1623–1629.
25 W. Tang, T. Zhang, Q. Li, H. Wang, H. Wang and Z. Li, *RSC advances*, 2016, **6**, 89888–89894.
26 F. Shen, C. Zhang, Z. Cai, Z. Qiu, Y. Wang, Z. Liu, M. Guan and F. Gao, *Chemical Engineering Journal*, 2022, **438**, 135556.
27 Y. Zhao, L. Zhou and Z. Tang, *Nature communications*, 2013, **4**, 1–8.
28 X. Zhang, C. Liu, L. Sun, X. Duan and Z. Li, *Chemical science*, 2015, **6**, 6213–6218.
29 Z. Cai, A. Wang, Y. Wang, Z. Qiu, Y. Li, H. Yan, M. Fu, M. Liu, Y. Yu and F. Gao, *Analytical Chemistry*, 2022, **94**, 9715–9723.
30 Y. Zhao, Y. Feng, Y. Zhang, P. Xia, Z. Xiao, Z. Wang and H. Yan, *Analytica Chimica Acta*, 2020, **1130**, 107–116.
31 A. J. Genot, T. Fujii and Y. Rondelez, *Journal of The Royal Society Interface*, 2013, **10**, 20130212.
32 L. E. Morrison and L. M. Stols, *Biochemistry*, 1993, **32**, 3095–3104.
33 L. E. Morrison and L. M. Stols, *Biochemistry*, 1993, **32**, 3095–3104.
34 E. Tan, B. Erwin, S. Dames, T. Ferguson, M. Buechel, B. Irvine, K. Voelkerding and A. Niemz, *Biochemistry*, 2008, **47**, 9987–9999.
35 H. Gudnason, M. Dufva, D. D. Bang and A. Wolff, *Nucleic acids research*, 2007, **35**, e127.

POSITIVE FEEDBACK DRIVES A SECONDARY NONLINEAR PRODUCT BURST DURING A BIPHASIC DNA AMPLIFICATION REACTION - ELECTRONIC SUPPLEMENTARY INFORMATION

BURCU ÖZAY,‡ SHANNON D. MURPHY,‡ ESTHER E. STOPPS, TOMÁŠ GEDEON, AND STEPHANIE E. MCCALLA*
‡AUTHORS CONTRIBUTED EQUALLY TO THIS WORK

Oligo Name	Sequence
LS2 template	5'-TCCGGA GAAT TAATGACTCT TCCGGA GAAT-3' NH_2
LS2 trigger	5'PO_3-ATTC TCCGGA-3'
LS2 dimer	5'PO_3-ATTC TCCGGA GAAT-3'
LS2 top strand	5'PO_3-ATTCTCCGGAAGAGTCATTAATTCTCCGGA-3'
LS2 20nt top strand	5'PO_3-ATTCTCCGGAAGAGTCATTA-3'
LS2 trigger A-tailed	5'PO_3-ATTC TCCGGA A-3'
LS3 lowpG3 template	5'-TCCGGA GTTTGG TAATGACTCT TCCGGA GTTTGG-3' NH_2
LS3 lowpG3 trigger	5'PO_3-CCAAAC TCCGGA-3'
LS3 lowpG3 dimer	5'PO_3-CCAAAC TCCGGA GTTTGG-3'
LS3 lowpG3 top strand	5'PO_3-CCAAACTCCGGAAGAGTCATTACCAAACTCCGGA-3'
LS3 lowpG3 22nt top strand	5'PO_3-CCAAACTCCGGAAGAGTCATTA-3'
LS3 lowpG3 trigger A-tailed	5'PO_3-CCAAAC TCCGGA A-3'
LS3 sp template	5'-CGCG GTTTGG TAATGACTCT CGCG GTTTGG-3' NH_2
LS3 sp trigger	5'PO_3-CCAAAC CGCG-3'
LS3 sp dimer	5'PO_3-CCAAAC CGCG GTTTGG-3'
LS3 sp top strand	5'PO_3-CCAAACCGCGAGAGTCATTACCAAACCGCG-3'
LS3 sp 20nt top strand	5'PO_3-CCAAACCGCGAGAGTCATTA-3'
LS3 sp trigger A-tailed	5'PO_3-CCAAAC CGCG A-3'
EXPAR1 template	5'-CTCACGCTAC GGACGACTCT CTCACGCTAC-3' PO_3
EXPAR1 trigger	5'-GTAGCGTGAG-3'

Table SI 1: Oligonucleotide sequences.

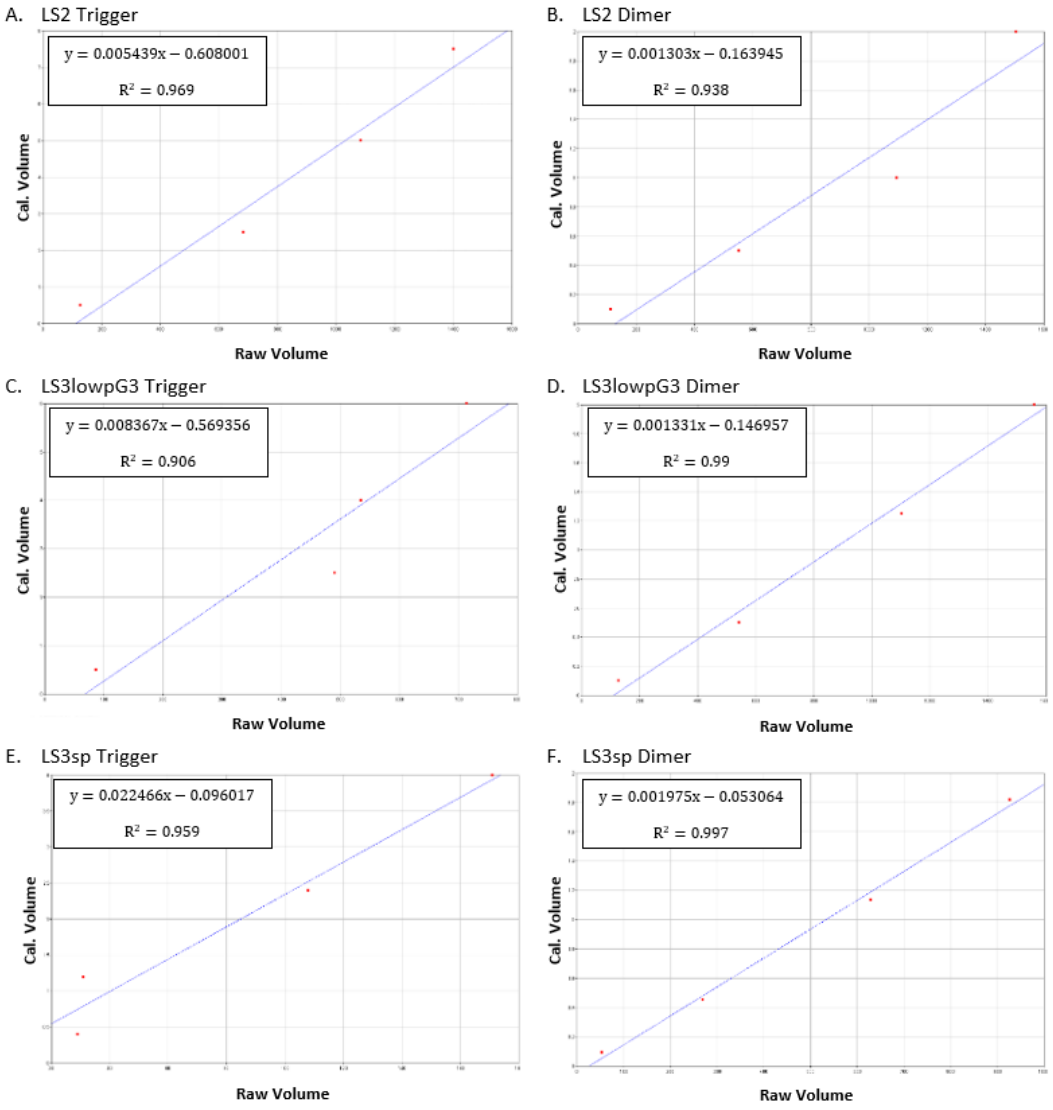

Figure SI 1: Example calibration curves of trigger and dimer standards for PAGE gel analysis, as calculated by GelAnalyzer 19.1 software (www.gelanalyzer.com).

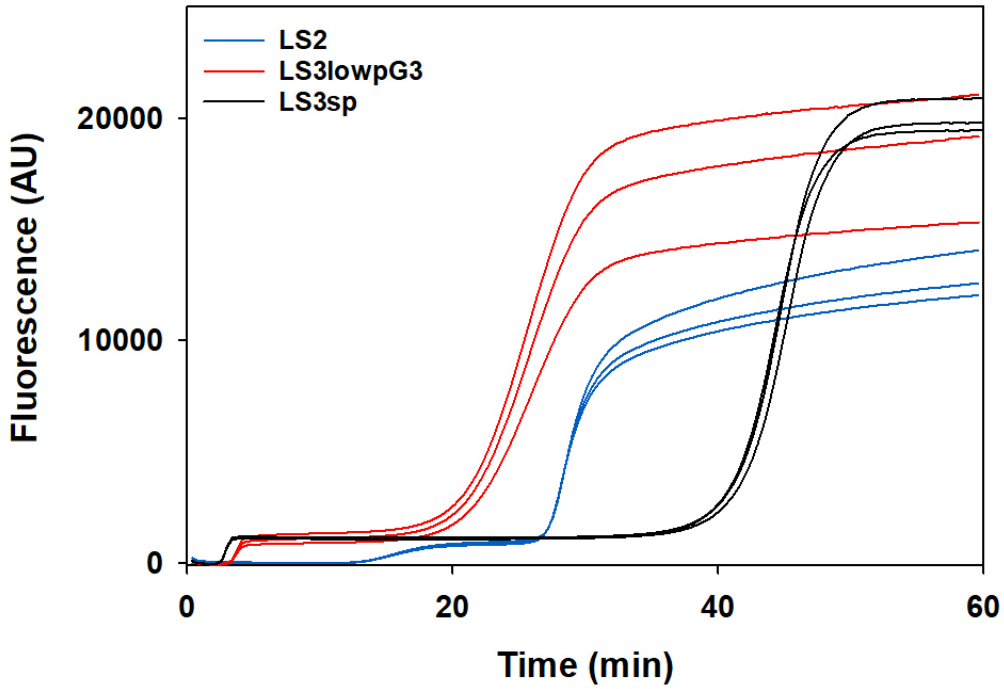

Figure SI 2: Fluorescence traces for three different templates shows the distinct biphasic response and large fluorescent output of UDAR. Three technical replicates from the same master mix are shown for each template.

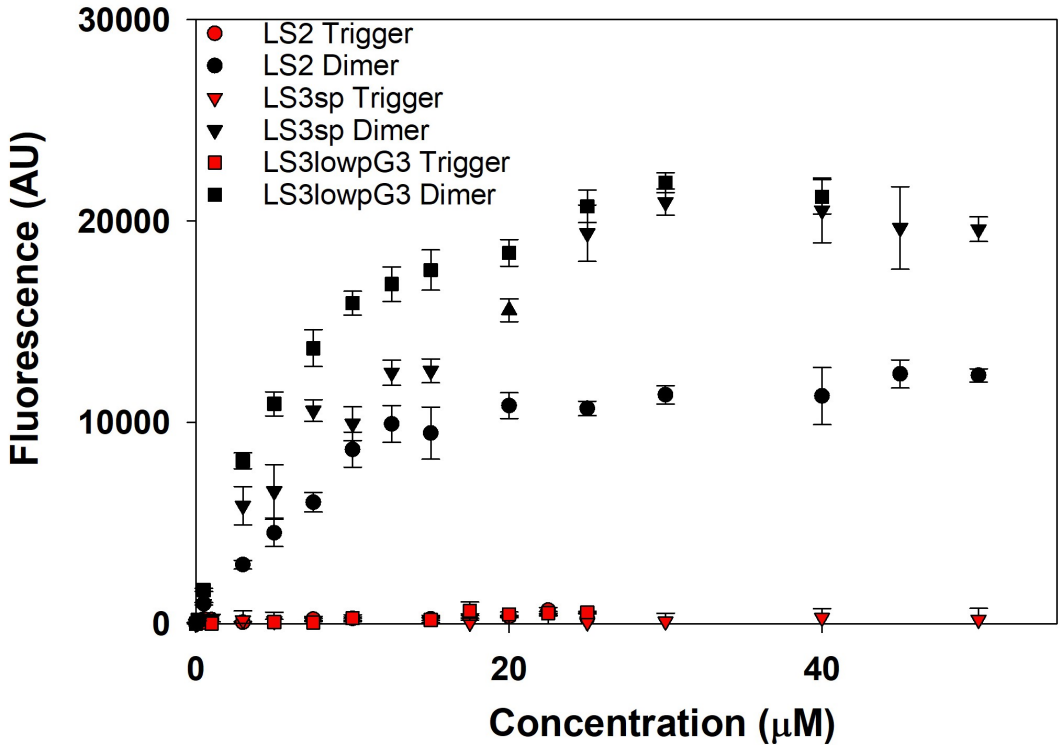

Figure SI 3: Staining performance of SYBR Green II for triggers and dimers of three different UDAR templates. Samples were prepared in UDAR buffer and fluorescence measurements were conducted by a qPCR machine at 55°C. While triggers provide minimal signal, extended trigger dimers and monomers $(S + D)$ create a significant fluorescent signal.

	κ_1	κ_2	k_1	k_2	κ_3
Second Phase Fit, LS2 and LS3lowpG	1,10^5	0.01,1	N/A	N/A	N/A
Second Phase Fit, LS3sp	1,10^{10}	0.01,2	N/A	N/A	N/A
Full Reaction, Initial Fit	N/A	N/A	10^{-5},100	$0.01, 10^4$	0.01,κ_2
Full Reaction, Final Fit	N/A	N/A	10^{-5},100	N/A	0.01,κ_2
Full Reaction, Final Fit, LS3sp	N/A	N/A	10^{-5},200	N/A	0.01,κ_2

Table SI 2: Constraints used during optimization with the MATLAB function fmincon.

[h]

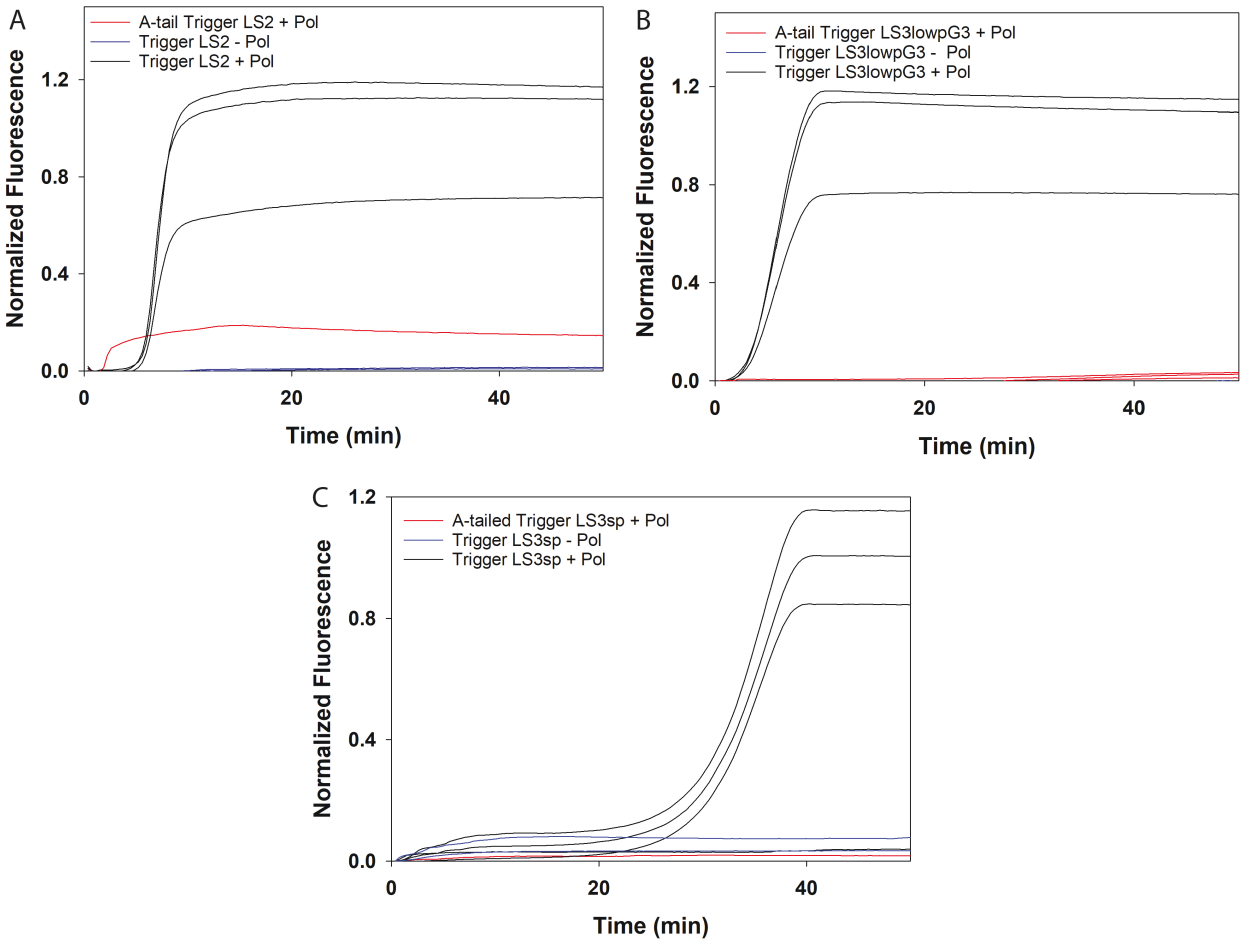

Figure SI 4: UDAR second phase reaction fluorescence traces for three different triggers and their A-tailed versions, with three technical replicates each from the same master mix. Samples with no polymerase added were included as background fluorescence controls. A-tailed triggers did not reproduce second phase production of highly fluorescent products. A-tailing of products by the polymerase was therefore not included in the mathematical model.

Computationally investigating polymerase association with double stranded DNA: It is possible that polymerase bound to double stranded DNA, which could decrease the unbound polymerase concentration in the reaction. We investigated this possibility by both including polymerase in the competition term for long double stranded DNA ($\kappa_3 = \kappa_4$), including polymerase in the competition term for all double stranded DNA ($\kappa_3 = \kappa_4 = \kappa_5$), or excluding polymerase from the competition term (κ_4 and κ_5 excluded). The model fits were optimal when using κ_4, although the model reproduces the reaction output without including sequestration of polymerase by double stranded DNA (Fig. SI 5 and Table SI 3). There were modest changes in the final fit parameters when these different competitive κ values were used (Table SI 4). It is possible that sequestration of polymerase by double stranded DNA did not need to be included in the final model, as the effect on the fit was modest.

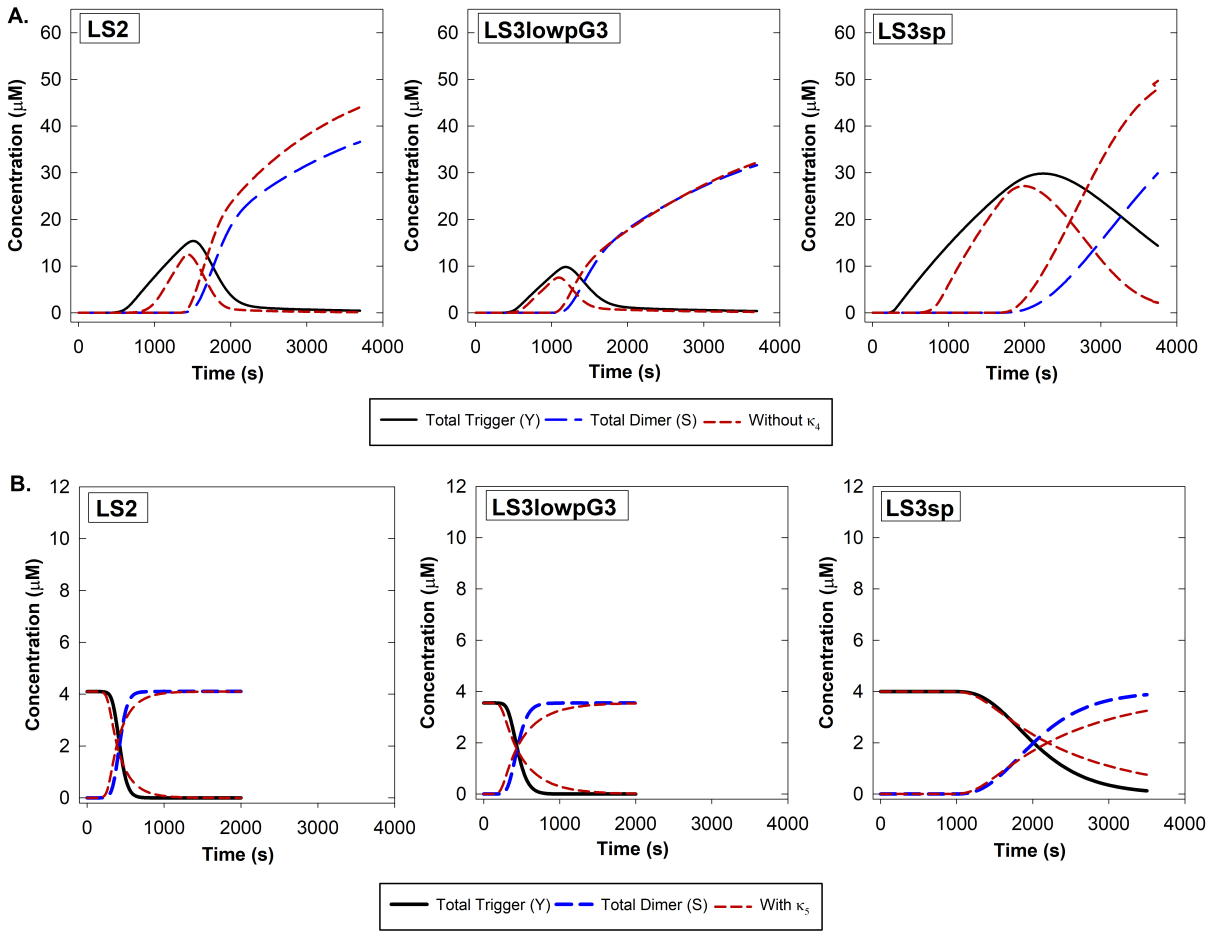

Figure SI 5: The effect of excluding polymerase rebinding to W and V (κ_4) in the full fit and including competition from double stranded dimer D (κ_5) in the second phase fit. A) Excluding κ_4, which acknowledges the possibility of Bst polymerase rebinding to fully dsDNA, results in a full fit that sill retains the rise and fall of Y and the steep second phase rise; however, the fit error increases. Therefore, κ_4 was included in the final model. B) Including competition from the double stranded dimer D (κ_5) also increases the model error and causes a decreased rate of second phase growth. Therefore, competition due to polymerase rebinding to D was not included in the final model.

	Final Full Fit	**Full fit without κ_4 (no dsDNA inhibition)**	**Final second phase fit**	**Second phase fit with κ_5 (ds Dimer inhibition)**
LS2	2.4E+04	4.4E+04	8.1	11.1
LS3lowpG3	5.9E+03	8.8E+03	11.6	14.0
LS3sp	4.0E+04	7.7E+04	105.0	122.5

Table SI 3: Comparison of least errors for fits using different assumptions for κ_4 and κ_5, which relate to polymerase rebinding to fully double stranded DNA.

Parameter	LS2	LS3lowpG3	LS3sp	
Full fit with κ_4				
k_1	7.6E-01	5.2E-02	2.6E-01	s^{-1}
k_2	2.6E+01	2.6E+01	2.6E+01	s^{-1}
κ_3	2.6E-02	5.8E-02	3.6E-02	μM
κ_4	2.6E-02	5.8E-02	3.6E-02	μM
Full fit without κ_4				
k_1	3.0E-01	4.8E-02	2.7E-02	s^{-1}
k_2	2.7E+01	2.7E+01	2.7E+01	s^{-1}
κ_3	1.0E-02	9.3E-02	1.0E-02	μM
κ_4	N/A	N/A	N/A	μM
Second phase fit without κ_5				
κ_1	1.0+04	1.0E+04	1.0E+06	μM
κ_2	3.5E-01	3.5E-01	8.9E-01	μM
Second phase fit with κ_5				
κ_1	5.0+03	1.0E+03	1.0E+06	μM
κ_2	3.0E-01	3.2E-01	8.1E-01	μM
κ_5	3.0E-01	3.2E-01	8.1E-01	μM

Table SI 4: Comparison of selected model parameters with and without simulated polymerase binding to fully double stranded DNA. The full fit with κ_4, as seen in the main text, is shown with the full fit without κ_4 for comparison. The inclusion of κ_4 assumes that the polymerase can rebind the fully double stranded template W. The second phase fit of κ_1 and κ_2, as seen in the main text, is compared with a fit that additionally includes κ_5. The inclusion of κ_5 assumes that the polymerase can rebind fully double stranded dimer D.

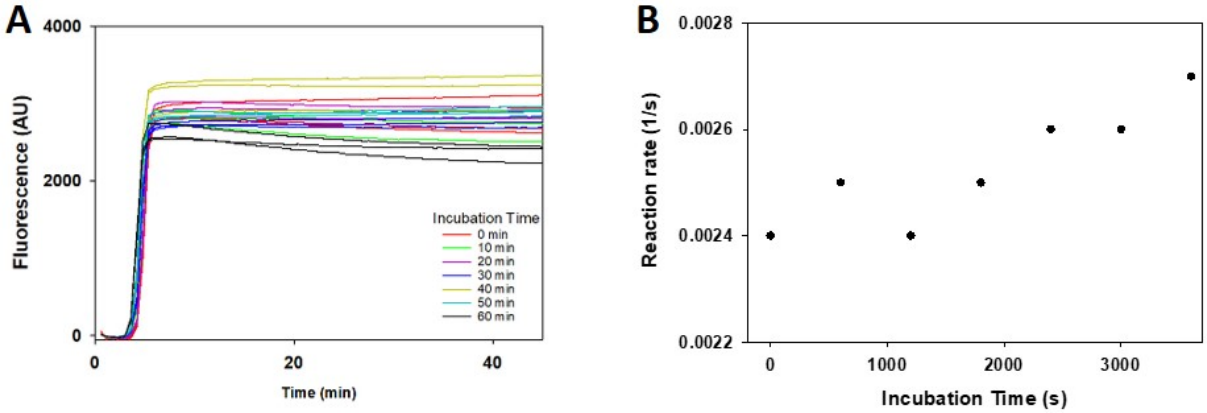

Figure SI 6: Polymerase activity did not notably change after 55°C incubation. A) Fluorescence-time traces of EXPAR samples, prepared with polymerase that was pre-incubated at 55°C. Six EXPAR reaction mixes were prepared with polymerase and without nicking endonuclease and template, and incubated for 0, 10, 20, 30, 50 and 60 min, respectively. Once the nicking endonuclease and an EXPAR template are added, 55°C incubation is continued and the fluorescence readings were performed every 24 seconds in a qPCR machine. B) The reaction rate, assumed to be a saturating exponential conversion between single stranded and double stranded template, minimally changes over time.

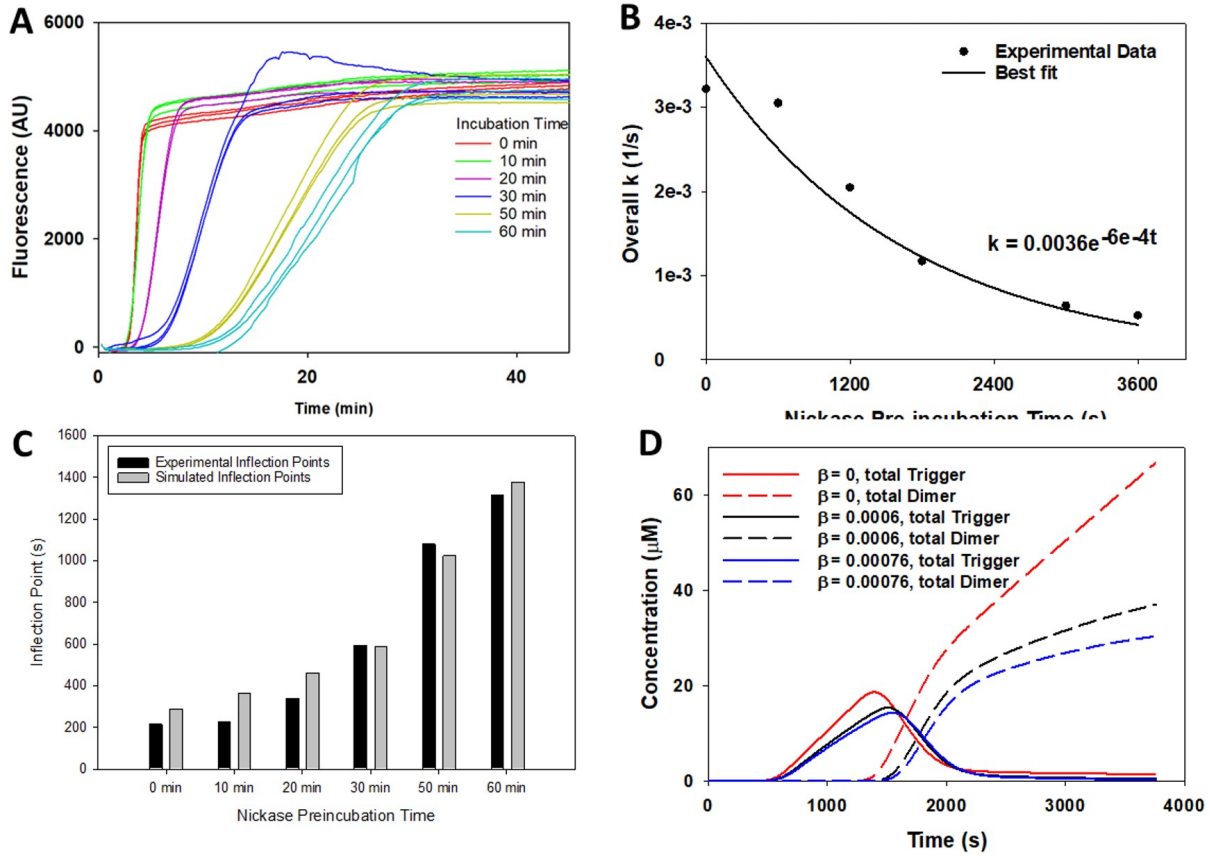

Figure SI 7: Nicking endonuclease activity changed over time with 55°C incubation. A) Fluorescence-time traces of EXPAR samples, prepared with nicking endonuclease that was pre-incubated at 55°C. Six EXPAR reaction mixes were prepared with nicking endonuclease and without polymerase and template, and incubated for 0, 10, 20, 30, 50 and 60 min, respectively. Once the polymerase and an EXPAR template are added, 55°C incubation is continued and the fluorescence readings were performed every 18 seconds in a qPCR machine. B) The reaction rate, assumed to be a saturating exponential conversion between single stranded and double stranded template, exponentially decreased over nickase incubation time.

Verifying nicking endonuclease deactivation: Nicking endonuclease slowly deactivates over time during EXPAR and UDAR reactions. To quantify this, nicking endonuclease was pre-incubated at 55°C for varying times in reaction buffer and then used in a subsequent EXPAR reaction (Fig. SI 7A). This reaction was originally assumed to fit the saturating exponential

$$F = F_{max}(1 - exp(-kt)),$$

where F_{max} is the maximum fluorescence, F is the fluorescence, and k is the overall reaction rate of the EXPAR reaction. The overall reaction rate is therefore $k = \frac{ln(2)}{IF}$, where the inflection point IF is assumed to approximate the point at which half of the maximum fluorescence occurs. The calculated overall reaction rate k exponentially decayed with pre-incubation time (Fig. SI 7B). The decay rate was taken as the model parameter β, which assumes that the overall reaction rate was proportional to the nicking rate $k_2[N]$. As this calculation carries several assumptions, we aimed to verify the validity of this calculation by fitting the inflection points found in a mathematical model of EXPAR with nicking endonuclease deactivation with our experimental data to extract β, and compare this value to the originally calculated β. The following

equations describe an EXPAR reaction:

$$\begin{aligned}
[\dot{Y}] &= -k_1(K_a[T][Y]) + k_2[N][W] \\
[\dot{W}] &= k_3[V] - k_2[N][W] + k_1(K_a[T][Y]) \\
[\dot{V}] &= -k_3[V] + k_2[N][W] \\
[\dot{N}] &= -\beta[N] \\
T &= T_0 - W - V
\end{aligned}$$

Here, T is the linear EXPAR template, T_0 is the initial concentration of template, W is fully double stranded template, V is nicked template, and $[N]$ is the nicking endonuclease. The parameter $K_a = 0.0694$ is the association constant of the EXPAR trigger calculated as described in the main text. The parameters $k_1 = 0.5s^{-1}$ and $k_2 = 25.75s^{-1}\mu M^{-1}$ were found in this study, and were the average value of the extension of a 10nt trigger bound to template and average overall nicking rate, respectively. The parameter k_3 describes extension of V to W. As with the original mathematical model introduced with EXPAR [1], we did not account for polymerase competition in this model. The observed increase in fluorescence during an EXPAR reaction is due to the single stranded template T becoming double stranded template W or V. We therefore define the species $T_d = W + V$, and find the ODE system:

$$\begin{aligned}
[\dot{Y}] &= -k_1(K_a[T][Y]) + k_2[N][W] \\
[\dot{T_d}] &= k_1(K_a[T][Y]) \\
[\dot{N}] &= -\beta[N] \\
T &= T_0 - T_d
\end{aligned}$$

We assume that $W \approx T_d$, as the two species should be similar in concentration; the species W is seen as the main template-derived product during the first phase of UDAR. The initial conditions were

$$N_0 = 0.026exp(-\beta t_p)$$

and $T_0 = 0.1$, where t_p is the pre-incubation time in seconds and T_0 is the initial concentration of template expressed in μM. We fit parameter β by minimizing the function

$$\sum_{i=1}^{n}(IF_i - \widehat{IF_i})^2$$

. Here, n is the number of pre-incubation data sets, IF_i is the experimentally determined inflection point found by numerically calculating the point where the second derivative of fluorescence is zero, and $\widehat{IF_i}$ is the inflection point in the rise of species T_d found in the second ODE model above. We constrained β to be between $0.0001 - 0.0008$. The resulting best fit value, $\beta = 0.000757$, differed from the original calculation by 26% and reproduced the inflection points across all pre-incubation times, including the EXPAR reaction that was not pre-incubated and therefore completed in less than 10 minutes (Fig. SI 7C). This difference minimally changes the output of the mathematical model (Fig. SI 7D), but the exclusion of β produces a large final product rise that is not seen in our reaction. We therefore maintained the original calculated value of $\beta = 0.0006$.

References

[1] J. Van Ness, L. K. Van Ness, and D. J. Galas, "Isothermal reactions for the amplification of oligonucleotides," *Proceedings of the National Academy of Sciences*, vol. 100, no. 8, pp. 4504–4509, 2003, ISSN: 0027-8424. DOI: 10.1073/pnas.0730811100. eprint: https://www.pnas.org/content/100/8/4504.full.pdf. [Online]. Available: https://www.pnas.org/content/100/8/4504.